Proximity Coupled Interdigitated Sensors to Detect Insulation Damage in Power System Cables

Rashed H. Bhuiyan, Roger A. Dougal, *Senior Member, IEEE*, and Mohammod Ali, *Senior Member, IEEE*

***Abstract*—Proximity coupled interdigitated sensors are introduced to detect insulation damage in power system cables. A new empirical model for interdigitated sensors with conducting backplane is developed. The validity of this newly proposed model is verified by comparing the results obtained from the new model with simulation and experimental results. It is shown that while the existing models fail to correspond to the simulation and experimental results due to the presence of the conducting backplane, the new model can fairly approximate the effect of the backplane on the sensor performance. A meander and a quarter-circular sensor are designed for insulation damage detection. Measurement results on planar dielectric materials, as well as practical power line cables are presented to demonstrate the usefulness of these sensors. Such sensors placed on microrobots crawling along power cables could lead to the potential autonomous monitoring of an electric power system.**

***Index Terms*—Fringing field, interdigitated sensor, nondestructive monitoring, penetration depth, water tree.**

I. Introduction

RELIABLE operation of an electric power system requires continuous or sporadic monitoring to detect and forecast aging status or faults in order to ensure optimum power system reconfiguration in real time. Cable insulation damage is a major problem in an electric power system. A void or hole present in the insulation may lead to severe faults like short-circuit and corona discharge. Furthermore, the presence of water or moisture can lead to the formation of water trees [1]–[3]. Cable failure generally occurs when water trees become electrical trees. For an established system, nonintrusive diagnosis is greatly preferred. During the last few decades, interdigitated sensors have been proposed for a diverse array of research and commercia1 applications ranging from smart (automated) control to moisture content measurement [4]. Proximity coupled capacitive sensors with an interdigitated structure are attractive candidates for nondestructive monitoring of the insulation status of a power system cable. The fringing near electric fields emanating from the interdigitated sensors enter the dielectric material of a cable. By measuring the interelectrode capacitance which is directly related to the relative permittivity of the insulation, the presence of void or water tree within the insulating material can be detected. Due to its inherent planar geometry, nondestructive monitoring is easily achieved by simply pressing the sensor against the solid material under test. In the literature, there are reports of robotic monitoring of power system using various sensors [5], [6]. One can envision that a microrobotic vehicle moves along a power line, places the planar sensor at different locations on the cable surface, takes measurement data, and wirelessly sends those to a central station where processing and decision making, such as power systems reconfiguration can take place.

For insulation damage detection, it is important to confine most of the electric field lines within the material under test. In that case, most of the field lines will generate at the driving electrode and terminate at the sensing electrode of the sensor. To ensure this, the substrate on which the sensor is printed should have a conducting backplane on the opposite side of the driving and sensing electrodes. Most of the analyses available in the literature on sensors with conducting backplane are generally qualitative in nature and, hence, do not properly explain the effect of the conducting backplane on the sensor performance. To accurately calculate the interelectrode capacitance of a sensor consisting of a conducting backplane, we need a new mathematical model which is validated by numerical simulations and experimental data. In this paper, we propose a new empirical model to calculate the interelectrode capacitance for the interdigitated sensor with a conducting backplane. To validate our proposed model, we compare results obtained from our proposed model with those obtained from Ansoft Maxwell simulation and experimental measurements. We also investigate the feasibility of using planar interdigitated sensors to detect voids or holes in a material by designing and testing a meander and a quarter-circular sensors. Experimental results on a number of dielectric materials, as well as practical power line cables are presented. One specific advantage of our quarter-circular sensor is its general immunity against the various orientations of a crack (orthogonal, parallel, or any arbitrary angle with respect to the electrode axis). This paper is organized as follows. In Section II, the basic operating principles of an interdigitated sensor is described, followed by a presentation of our proposed new empirical model in Sections III and IV. Finally, in Sections IV and V, we present experimental data on a number of dielectric materials and practical power line cables.

II. Basic Operating Principle and Design

A. Effective Dielectric Constant

A proximity coupled interdigitated sensor applies a periodic electrical potential to the surface of the test material and measures the fringing electric field capacitance. Physical changes in the insulating material are usually reflected in the change of

Manuscript received May 11, 2007; revised July 27, 2007; accepted August 9, 2007. This work was supported in part by the U.S. Office of Naval Research under Grant N00014-02-1-0623. The associate editor coordinating the review of this paper and approving it for publication was Prof. Fabien Josse.

The authors are with the Department of Electrical Engineering, University of South Carolina, Columbia, SC 29208 USA (e-mail: bhuiyan@engr.sc.edu; dougal@engr.sc.edu; alimo@engr.sc.edu).

Color versions of one or more of the figures in this paper are available online at http://ieeexplore.ieee.org.

Digital Object Identifier 10.1109/JSEN.2007.908440

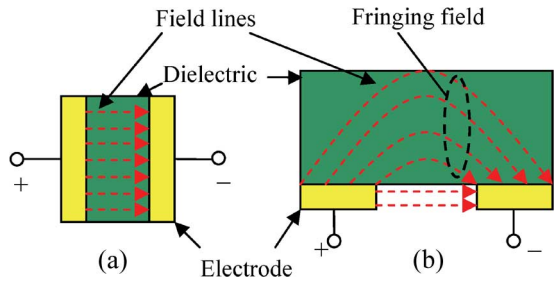

Fig. 1. (a) Parallel plate capacitor. (b) Interdigitated capacitor.

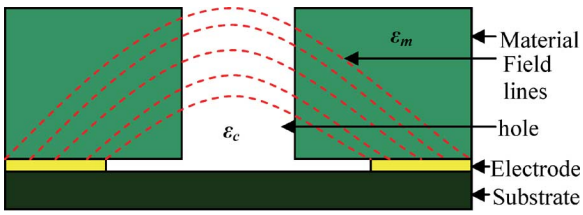

Fig. 2. A damaged material on a pair of electrodes.

the dielectric property. The basic geometries of a parallel plate and an interdigitated capacitor are compared in Fig. 1. Unlike a parallel plate capacitor, in an interdigitated capacitor, the plates are co-planner in nature. As shown in Fig. 1, for a parallel plate capacitor, the field line length is equal to the geometric (linear) distance between the plates. However, for an interdigitated capacitor, the field line length is not equal to the linear distance between the plates. This is because in addition to direct field lines between the plates, there are bent or fringing field lines, as seen in Fig. 1(b). So, for the latter case, an average of the lengths of all fields should be considered.

If the insulating material of a power line cable has a void or hole within it, then air or water intrusion can easily occur. In the presence of an interdigitated sensor, such a scenario can be considered to be similar to a multilayer dielectric capacitor. The effective dielectric constant of a multilayer dielectric capacitor can be calculated using the expression given in [7]. Fig. 2 shows a damaged material placed on top of a pair of electrodes. Let the average length of the electric field lines traversing the material above the electrode pair is h_t and the average length of the electric field lines traversing the crack is h_c. Relative permittivity of the material is ε_m and that of the crack is ε_c. Then, an approximate expression for the effective dielectric constant

$$\varepsilon_{eff} = \frac{h_t}{\frac{h_m}{\varepsilon_m} + \frac{h_c}{\varepsilon_c}} \tag{1}$$

where $h_m = h_t - h_c$

From this relation, it is seen that the effective dielectric constant depends on the length and permittivity of the material trapped in the crack. Since capacitance depends on dielectric constant, capacitance of damaged insulation is different from its undamaged counterpart.

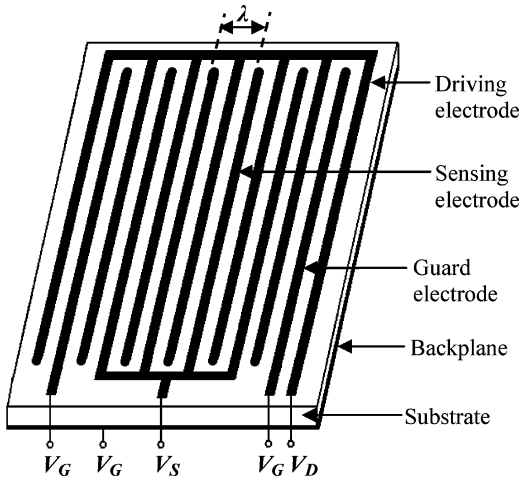

Fig. 3. Typical geometry of an interdigitated sensor.

B. Basic Sensor Geometry and Circuit

Fig. 3 shows the typical geometry of an interdigitated sensor, as described in [4]. During practical usage, the top surface of the sensor is brought in contact with the material under test. There are three types of electrodes, namely, driving electrodes, sensing electrodes, and guard electrodes. These electrodes are mounted on an insulating substrate. There is a conducting layer on the backside of the substrate called the backplane. A sinusoidal signal (V_D) is applied to the driving electrode and the output signal (V_S) is measured at the sensing electrode. The backplane and guard electrodes (which are usually kept at ground potential V_G) remove any unwanted external field influences [4], [8]. The backplane restricts unwanted radiation of field in the backward direction. The most important dimension of the sensor is its spatial wavelength (λ) (distance between the same types of electrodes). The spatial wavelength determines the penetration depth of the electric field lines into the material under test. The penetration depth is approximately equal to 1/3 of the spatial wavelength [9], [10].

Material properties are measured using the short-circuit current method [10]–[12], as shown in Fig. 4(a). This method increases the resolution, simplifies the equivalent circuitry, and is more robust to noise. In this method, the driving electrode is excited by a low-frequency sinusoidal voltage V_D, the sensing electrode is virtually grounded by an opamp, and the opamp output voltage (V_F) is measured across a known feedback capacitor (C_F).

A simplified equivalent circuit shown in Fig. 4(b) can be used for the calculation of the capacitance between the driven and the sensing electrodes. Here, C_{DG} represents the capacitance between the driving electrode and the grounded backplane and C_{DS} is the capacitance between the driving and sensing electrodes, which depends on the dielectric constant of the test material. Most insulating materials have nearly infinite resistance, so the current is solely due to the capacitive reactance. Taking the summation of the currents at the virtually grounded node it can be shown that

$$C_{DS} = \frac{V_F}{V_D} C_F. \tag{2}$$

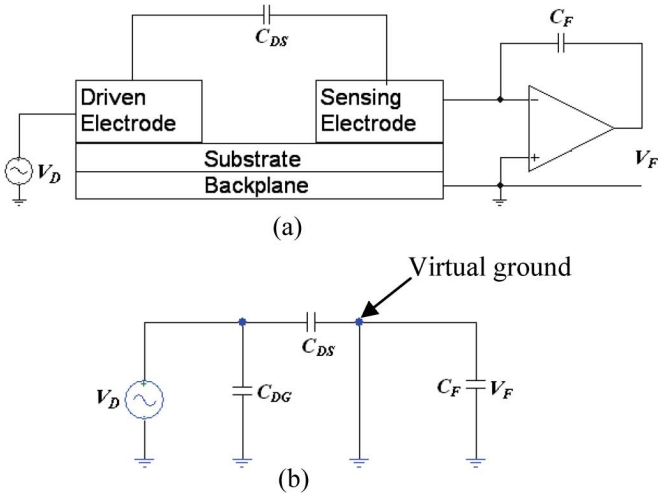

Fig. 4. (a) Block diagram of sensor circuit and its (b) equivalent.

III. A New Empirical Model of the Interdigitated Sensor

Accurate analytical model of interdigitated sensors is currently not available simply due to the complicated nature of the fields. An approximate formula based on the conformal mapping method was proposed in [13] and [14] to calculate the capacitance C_{DS} between the driven and the sensing electrodes.

Fig. 5 shows a unit cell (UC) of an interdigitated sensor without a conducting backplane. Here, the electrode width is half of the real width. If C_m and C_s is the per unit capacitance of the material under test and the substrate, respectively, then the per unit capacitance of the sensor can be found as [13]

$$C_{ms} = \varepsilon_0 \frac{(\varepsilon_m + \varepsilon_s)}{2} \frac{K\left[\sqrt{\left\{1-\left(\frac{a}{b}\right)^2\right\}}\right]}{K\left[\frac{a}{b}\right]} \tag{3}$$

where C_{ms} is the sum of C_m and C_s and $K[\sqrt{\{1-(a/b)^2\}}]$ and $K[a/b]$ are the complete elliptic integrals of modulus $\sqrt{\{1-(a/b)^2\}}$ and (a/b), respectively. If the trapped material within the interelectrode gap has a capacitance of C_a, then from [14]

$$C_a = \varepsilon_0 \varepsilon_a \frac{h}{a}. \tag{4}$$

The total per unit capacitance of the sensor is given by

$$C_{PU} = C_{ms} + C_a. \tag{5}$$

If the electrode length is L and the total width is W, as shown in Fig. 6, then the total capacitance is given by

$$C_{DS} = \left(\frac{W-b}{2b}\right) L C_{PU}. \tag{6}$$

The above equations do not include the effect of a conducting backplane and also assumes that the field penetration depth is equal to the substrate thickness. As mentioned before, for insulation damage detection interdigitated sensors with conducting backplane are required to ensure that most of the field lines

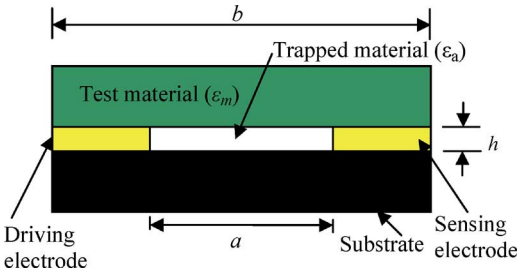

Fig. 5. Unit cell representation of interdigitated sensor.

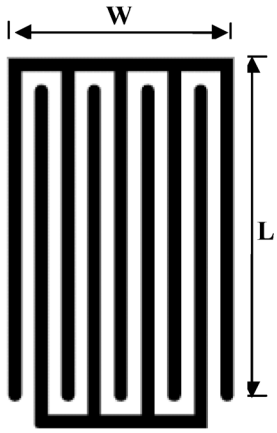

Fig. 6. Electrode dimensions.

are confined within the material under test instead of leaking through the back side of the substrate. Furthermore, it is greatly desired that the sensor substrate be very thin and preferably flexible to allow it for easy placement on a curved surface, such as a cable. This will clearly make the field penetration depth much larger than the substrate thickness.

Due to the inherent difficulty in developing exact analytical formulas for such a complicated geometry, we propose an empirical equation based on our simulation and measurement results on a number of materials. Most of the field lines penetrate the material under test and travel from the driving electrode to the sensing electrode. The use of a low dielectric constant material as the substrate for the sensor further helps field concentration within the material under test. As the substrate thickness is small, the driving and sensing electrodes are in close proximity to the conducting backplane. This ensures that the electric field lines that penetrate the substrate end at the backplane instead of the sensing electrode. The field lines between the electrode and the backplane are responsible for the substrate capacitance which has no contribution to the interelectrode capacitance C_{DS}. Therefore, neglecting the contribution from the substrate capacitance and modifying (5)

$$C_{PUc} = A\varepsilon_0 \left[\frac{\varepsilon_m}{2} \frac{K\left[\sqrt{\left\{1-\left(\frac{a}{b}\right)^2\right\}}\right]}{K\left[\frac{a}{b}\right]} + \varepsilon_a \frac{h}{a}\right] \tag{7}$$

where C_{PUc} is the corrected per unit capacitance and A is a correction factor which corresponds to the redistribution of the

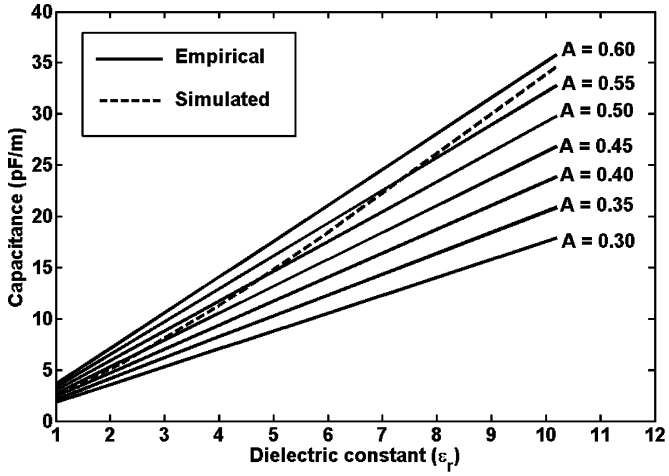

Fig. 7. Estimating A for the sensor with a conducting backplane.

field lines of C_m and C_a. As discussed in Section IV-A, A can be calculated as

$$A = p\varepsilon_m + 0.4 \tag{8}$$

where p is a constant whose value is estimated based on Maxwell simulations. The total interelectrode capacitance can be found by replacing C_{PU} in (6) by C_{PUc} in (7).

IV. Results

A. Empirical Model and Simulation Results

Maxwell 2-D was used to simulate the sensor response. A unit cell, as shown in Fig. 5, was considered for samples with dielectric constants ranging from 1 to 11. However, unlike the structure in Fig. 5, our simulation model consisted of a conducting backplane. The simulation results are compared with the results obtained using our proposed simple model (7). In Fig. 7, the dashed line represents the simulation results, while the solid lines represent results obtained using our proposed equation for various A values. It is observed that for sample dielectric constant values between 1 and 3, the dashed simulation curve is between the empirical curves labeled $A = 0.4$ and $A = 0.45$. For dielectric constants ranging from 3 to 5, the simulation curve is between curves labeled as $A = 0.45$ to $A = 0.5$. Similarly, considering other regions of the curves and corresponding dielectric constants, we clearly see that A must be at least 0.4 and increase proportionally with the dielectric constant of the sample which is estimated in (8).

For most practical power line cables, the dielectric constant is low and rarely exceeds 10. For instance, Kynar used as cable insulation has the highest dielectric constant which is 8.4 at 60 Hz [15]. So, it is reasonable to choose dielectric constant ranging from 1 to 10. For this range, an approximate value of p can be chosen as 0.02. Table I summarizes values of capacitance per meter for six different samples. It is seen that for a sensor without a conducting backplane the capacitance calculated using (5) and listed in column 4 agrees well with the simulated capacitance listed in column 3. By contrast, for a sensor with a conducting backplane, the simulation results obtained using Maxwell and listed in column 5 are quite different from those listed in column 4. This is due to the fact that the model in (5) does not include the effect of the backplane. In column 6 of Table I, we have listed capacitance data calculated using our proposed empirical model. As apparent from the results, in the presence of the conducting backplane, our proposed model is in good agreement with the Maxwell simulation results (in column 5).

TABLE I
Interelectrode Capacitance Data of an Interdigitated Sensor

Sample Material	Relative Dielectric constant (ε_r)	Sensor without a conducting backplane		Sensor with a conducting backplane	
		Capacitance from Maxwell Simulation (pF/m)	Capacitance using equation (5), [13]-[14], (pF/m)	Capacitance from Maxwell Simulation (pF/m)	Capacitance from our proposed model (pF/m)
Air	1.0006	17.06	18.79	2.39	2.5
PTFE	2.2	22.46	25.78	5.56	5.75
PVC	4.0	30.47	36.28	11.27	11.26
FR4	4.4	32.25	38.6	12.64	12.58
Polyurethane	6.0	39.35	47.93	18.38	18.26
Duroid 6010	10.2	57.96	72.42	34.59	35.99

Fig. 8. Photographs of the (a) meander sensor, (b) quarter-circular sensor, and (c) sensor backplane.

B. Sensor Design for Damage Detection in Materials

To explore the prospects of detecting voids or holes in a dielectric material and also subsequently detect the damage on the insulation of a power line cable, we designed and fabricated two interdigitated sensors. The photographs of the two sensors, the meander and the quarter-circular sensor are shown in Fig. 8. The quarter-circular sensor was designed for rotation insensitive measurements, which means due to its geometry the measured interelectrode capacitance data for a particular sample should be generally less sensitive when the sensor is rotated on the measurement sample.

Each of the above two sensors was used to perform measurements on three types of dielectric materials, PTFE, FR4, and Duroid 6010. At first, measurements were done on undam-

Fig. 9. Sample 1.5-mm-thick damaged Duroid 6010.

TABLE II
MEASURED CAPACITANCE, C_{DS} (pF) DATA USING THE MEANDER SENSOR ON UNDAMAGED SAMPLES

Test Material	Measured Capacitance (pF)			
	Position 1	Position 2	Position 3	Average
Air	0.6	0.72	0.81	0.71
PTFE	1.04	1.16	1.17	1.12
FR4	2.13	2.26	2.22	2.2
Duroid 6010	5.35	5.23	5.23	5.27

TABLE III
MEASURED CAPACITANCE C_{DS} (pF) DATA FOR QUARTER-CIRCULAR SENSOR ON UNDAMAGED SAMPLES

Test Material	Measured Capacitance (pF)			
	Position 1	Position 2	Position 3	Average
Air	0.96	0.83	1.08	0.96
PTFE	1.15	1.23	1.24	1.21
FR4	1.9	1.83	1.75	1.83
Duroid 6010	4.88	4.2	4.45	4.51

aged samples followed by measurements on samples with a 12 mm × 6 mm hole. Fig. 9 shows the photograph of a Duroid 6010 sample material with a hole. To characterize the material under test, the sensor was placed on the sample such that the sensor's backplane was facing up and the sensor's top surface was in intimate contact with the sample. A 1 kHz sinusoidal signal was applied as the driving voltage. This low-frequency signal is easy to generate, and it ensured no additional shielding requirement, especially from the 60 Hz power line signal. The amplitude of the 1 kHz signal was chosen to be 10 V to prevent the opamp from saturation. This also ensured a high enough output signal above the noise level. A 100 pF capacitor was used as the reference capacitor (C_F). This value of C_F gives a measurable output voltage, while preventing the opamp from saturating. A piece of 10 mil thick Duroid 5880 $(\varepsilon_r = 2.2)$ substrate was used to fabricate the sensor. The spatial wavelength (λ), electrode width, height and gap were 4.5 mm, 1.125 mm, 17 μm, and 1.125 mm, respectively.

Tables II and III show the interelectrode capacitance, C_{DS} data measured for undamaged samples using the meander

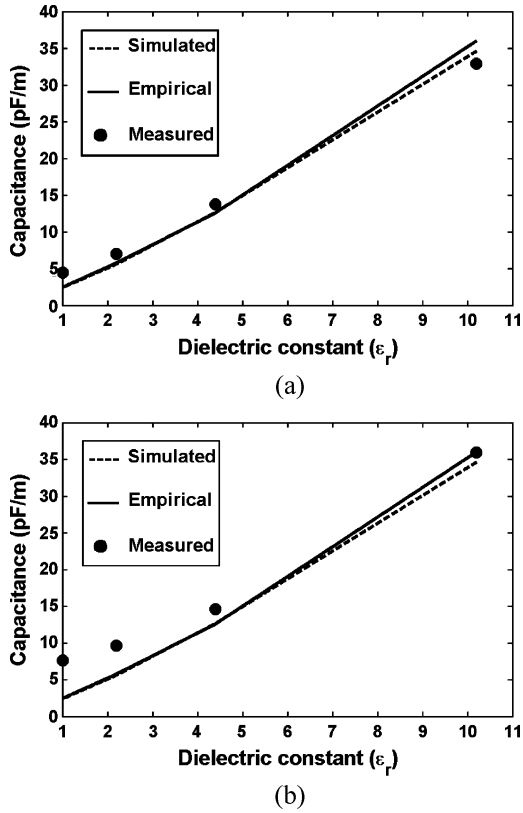

Fig. 10. Comparison of simulated, empirical and measured capacitance for the (a) meander and (b) quarter-circular sensors.

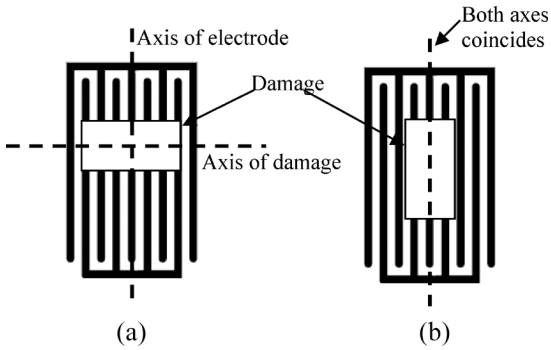

Fig. 11. Illustration of (a) orthogonal and (b) parallel damage.

and quarter-circular sensors, respectively. Measurements were taken at three different locations on the sample surface, and then an average of the data was taken. Simulated, empirical, and measured C_{DS} values are compared in Fig. 10. The measured data are in good agreement with the empirical and simulated results.

While measuring damaged materials, the orientation of the voids or holes may be parallel or orthogonal (perpendicular) with respect to the electrode axis (see Fig. 11). The cracks/holes may also form arbitrary angles with respect to the electrode axis. In these cases, C_{DS} can vary significantly because the dielectric constant will depend on the length of the damage which is traversed by the electric field lines. A circular sensor will be largely immune to this problem because of its geometry. Next, measurements were taken on damaged materials using

TABLE IV
MEASURED CAPACITANCE C_{DS} (pF) DATA FOR MEANDER SENSOR ON DAMAGED SAMPLES

Test Material	Parallel damage			Aver-age	Orthogonal damage			Aver-age
	Posit-ion 1	Posit-ion 2	Posit-ion 3		Posit-ion 1	Posit-ion 2	Posit-ion 3	
PTFE	0.8	0.85	0.82	0.82	0.78	0.81	0.79	0.79
FR4	1.26	1.29	1.27	1.27	1.2	1.13	1.2	1.18
Dur-oid 6010	3.71	3.86	3.97	3.85	3.39	3.22	3.36	3.3

TABLE V
MEASURED CAPACITANCE C_{DS} (pF) DATA FOR QUARTER-CIRCULAR SENSOR ON DAMAGED SAMPLES

Test Material	Measured Capacitance (pF)			
	Position 1	Position 2	Position 3	Average
PTFE	0.99	0.98	0.99	0.99
FR4	1.48	1.48	1.49	1.48
Duroid 6010	2.99	3.39	3.96	3.45

the meander sensor. The sensor surface was rotated with respect to the damage and measurements were taken for two extreme cases, parallel and orthogonal. These results are shown in Table IV, where we can see that when the axis of damage in a PTFE substrate is parallel with respect to the electrode axis, the sensor output is 0.82 pF, whereas when the same damage is orthogonal, the sensor output changes to 0.79 pF. Similarly for Duroid 6010, the sensor gives 3.85 pF for parallel damage and 3.3 pF for orthogonal damage. It appears that the meander sensor is sensitive to the damage orientation particularly for materials with higher dielectric constants. Measurement data obtained using the quarter-circular sensor are listed in Table V. It is observed that the quarter-circular sensor gives 0.99 pF and 3.45 pF for PTFE and Duroid 6010 substrates, respectively. Due to the finger geometry, there is no parallel or orthogonal orientation of the damage with respect to the electrode axis. Measurements taken by rotating the sensor with respect to the damage yielded consistently similar results ensuring that the quarter-circular sensor is insensitive to the orientation of the damage.

To evaluate the effect of air intrusion into the damaged location, we can compare the data in Table II with those in Table IV. Both of these two data tables represent the meander sensor. For instance, for undamaged PTFE, C_{DS} is 1.12 pF as opposed to 0.82 pF for parallel or 0.79 pF for orthogonal damage. Similarly, for FR4 and Duroid 6010, the values of C_{DS} with no damage are 2.2 pF and 5.27 pF, respectively, while those with damage are 1.27/1.18 pF and 3.85/3.3 pF, respectively. Clearly, the presence of a damage decreases the capacitance between the driven and the sensing electrodes. We observe a very similar trend when we compare Tables III and V each of which represents measured data using the quarter-circle sensor. Measured C_{DS} for PTFE, FR4, and Duroid 6010 with no damage are 1.21, 1.83, and 4.51, while those for the same material with damage are 0.99, 1.48, and 3.45, respectively.

TABLE VI
MEASURED CAPACITANCE C_{DS} (pF) DATA FOR PUR CABLE

Damage Type	Measured Capacitance (pF)			
	Position 1	Position 2	Position 3	Average
No damage	1.243	1.226	1.406	1.292
Air filled hole	0.812	0.784	0.857	0.818
Water soaked foam in hole	8.288	8.01	8.848	8.382

TABLE VII
MEASURED CAPACITANCE C_{DS} (pF) DATA FOR PVC CABLE

Damage Type	Measured Capacitance (pF)			
	Position 1	Position 2	Position 3	Average
No damage	1.042	1.047	1.109	1.066
Air filled hole	0.392	0.448	0.487	0.442
Water soaked foam in hole	6.272	6.72	7.392	6.795

V. MEASUREMENT OF INSULATION DAMAGE ON A POWER LINE CABLE

In our previous discussions, we have developed models and performed measurements for the interdigitated sensor for test samples which are planar in nature. However, in practical power systems if a cable needs to be monitored, its surface will be essentially curved and the sensor design must be focused in that direction so that it can be properly placed on the cable surface. We obtained two types of power line cables from SAB North America [16]- Polyvinylchloride (PVC) insulated cable ($\text{diameter} = 34.3\ \text{mm}$, $\text{insulation thickness} = 5.5\ \text{mm}$) and Polyurethane (PUR) insulated cable ($\text{diameter} = 26.7\ \text{mm}$, $\text{insulation thickness} = 4.5\ \text{mm}$) having dielectric constants of 4.0 and 6.0, respectively.

To properly place the sensor on one hemicylindrical surface of the cable, generally the sensor's finger length should be small. We designed a sensor with finger length of 10 mm. Then, the sensor was placed on the cable where the driving and sensing electrodes came in intimate contact with the cable's surface. To ensure that there was no air gap between the sensor and the cable surface, a vise was used to hold the sensor to the cables surface.

First, measurements were taken on the cable without any damage. Then, 12 mm × 6 mm holes were created on different places of the cable insulation and a number of measurements were taken. To measure the presence of materials other than air in the damaged location, a small piece of foam soaked in water was also inserted in the hole and measurements were taken.

Tables VI and VII list the measurement data for the PUR and PVC cables, respectively. From Table VI, it is observed that the presence of damage on the PUR cable insulation reduces the capacitance C_{DS} by 36.7%. The presence of water in the damage, on the other hand, increases C_{DS} significantly (548.9%). Similarly, for the PVC cable, the presence of a damage reduces C_{DS} by 58.5%, while the presence of water in the damage increases C_{DS} by 537.4%. So, from the sensor output, the existence of damage on cable insulation and the presence of air, water, or other materials in the damage can be detected. Even though the

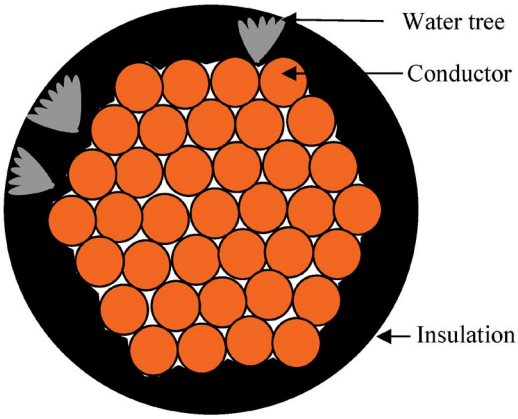

Fig. 12. Illustration of water tree presence in a power line cable.

dimensions of the hole/void considered here is relatively large and, hence, may seem plausible that they can be inspected visually, the proposed technique is advantageous because the alternative of monitoring visually can be very expensive.

Also, as mentioned earlier, another problem commonly encountered with aging power line cables is the formation of water trees due to the presence of moisture or water. In cable insulation, tiny channels may grow up in the presence of water. These water filled channels increase rapidly in number and create leafless bush like structure called water tree, as shown in Fig. 12. The dimension of a water tree varies from a fraction of a millimeter (mm) to several mm [1], [17], [18]. To artificially generate an approximate water tree test case, we created 16 adjacent cylindrical holes on the two cables (PUR and PVC). The holes were 1 mm in diameter and 1 mm in length. Prior to measurement, we filled the holes with water. A transparent scotch tape was placed on top of the holes to retain the water. Such test cases were developed on six different locations for each cable.

The bar diagrams in Fig. 13 show the measurement data on the two cables. It is apparent that there are some variations between the measured C_{DS} data at different locations on the cables. This can be attributed to the differences in hole sizes and the water present in the holes. Nevertheless, in all test cases the C_{DS} is always larger when measurements were taken on top of water filled holes.

Since sensor response varies at different locations, we propose here a concept of threshold capacitance level. From the readings on the PVC cable at six different locations illustrated in Fig. 13(a), we see that in the presence of tiny water filled holes, the readings are always above 3 pF, which can be considered as the threshold level (indicated using the dashed straight line in Fig. 13). For PUR cable, the threshold level is 3.5 pF, as seen in Fig. 13(b). The higher C_{DS} value for the PUR cable results from the higher dielectric constant of the PUR insulation. Thus clearly, the presence of small millimeter sized waterfilled holes can be easily detected using the proposed interdigitated sensors.

VI. Conclusion

The potential of a proximity coupled interdigitated sensor for insulation damage detection in power system cable was studied. A new empirical model to analyze a sensor backed by a conducting backplane was proposed. Results obtained using the proposed model are in very good agreement with the results obtained from Ansoft Maxwell simulation and experimental measurements. A meander and a quarter-circular sensors were designed to explore the feasibility of insulation damage detection. It was observed that with both types of sensors, the presence of a void within a dielectric substrate was easily detectable from the measured interelectrode capacitance data. Finally, a sensor was designed to detect the insulation damage of a power line cable. The measurement data confirms that the sensor can indicate the presence of holes and water trees in a power line cable. Although all measurements were done considering a static platform for the sensor, we can envision that a microrobotic vehicle moves along the cable surface, places the sensor and performs the measurement. However, for voids or water tree damages that are extremely small (micrometer in dimension and just about forming) in size or do not contain enough water or moisture, the change of dielectric constant at the damaged location may not be significant enough to ensure proper detection. Hence, future research is needed in advanced sensor design that will enable one to detect extremely small damaged areas or water trees that are about to form on power line cables.

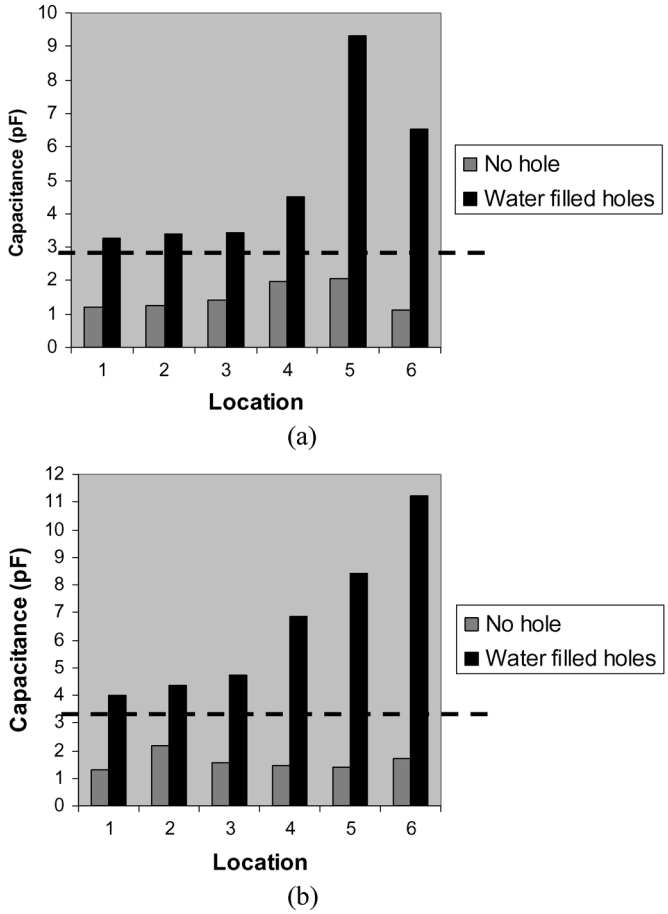

Fig. 13. Measured capacitance profile of a (a) PVC cable and (b) PUR cable with waterfilled small holes.

References

[1] E. F. Steennis and F. H. Kreuger, "Water treeing in polyethylene cables," *IEEE Trans. Electr. Insul.*, vol. 25, no. 5, pp. 989–1028, Oct. 1990.

[2] R. Ross, "Inception and propagation mechanisms of water treeing," *IEEE Trans. Dielectr. Electr. Insul.*, vol. 5, no. 5, pp. 660–680, Oct. 1998.
[3] T. A. Short, *Electric Power Distribution Handbook*. Boca Raton, FL: CRC, 2004, p. 139.
[4] A. V. Mamishev, K. Sundara-Rajan, F. Yang, Y. Du, and M. Zahn, "Interdigital sensors and transducers," *Proc. IEEE*, vol. 92, no. 5, pp. 808–845, May 2004.
[5] B. Jiang and A. Mamishev, "Robotic monitoring of power systems," *IEEE Trans. Power Delivery*, vol. 19, no. 3, Jul. 2004.
[6] B. Jiang, R. M. Wistort, and A. V. Mamishev, "Autonomous robotic monitoring of underground cable systems," in *Proc. 12th Inter. Conf. Adv. Robot.*, Jul. 2005, pp. 673–679.
[7] B. C. Wadell, *Transmission Line Design Handbook*. Norwood, MA: Arctech House, 1991, p. 417.
[8] M. Mehregany, P. Nagarkar, S. D. Senturia, and J. H. Lang, "Operation of micro-fabricated harmonic and ordinary side-drive motors," in *Proc. IEEE Micro Electro Mecha. Syst. Workshop*, 1990, pp. 1–8.
[9] N. F. Sheppard, Jr., "Design of a conductimetric microsensor based on reversibly swelling polymer hydrogels," in *Proc. 6th Int. Conf. Solid-State Sensors Actuators (Transducers'91)*, San Francisco, CA, Jun. 1991, pp. 773–776.
[10] Y. Du, "Measurements and modeling of moisture diffusion processes in transformer," Ph.D. dissertation, Dept. Elect. Eng. Comput. Sci., Mass. Inst. Technol., Cambridge, MA, 1999.
[11] M. C. W. Coln, "A high performance dielectric measurement system," Ph.D. dissertation, Dept. Elect. Eng. Comput. Sci., Mass. Inst. Technol., Cambridge, MA, 1985.
[12] A. V. Mamishev, "Interdigital dielectrometry sensor design and parameter estimation algorithms for non-destructive materials evaluation," Ph.D. dissertation, Dept. Elect. Eng. Comput. Sci., Mass. Inst. Technol., Cambridge, MA, 1999.
[13] R. Y. Scapple, "A trimmable planar capacitor for hybrid applications," in *Proc. 24th Electron. Compo. Conf.*, 1974, pp. 203–207.
[14] E. Endres and S. Drost, "Optimization of the geometry of gas-sensitive interdigital capacitors," *Sens. Actuators B, Chem.*, vol. 4, pp. 95–98, 1991.
[15] C & M Corporation, "Insulation materials properties chart." [Online]. Available: http://www.cm-corp.com
[16] [Online]. Available: http://www.sabcable.com
[17] A. A. Al-Arainy, A. A. Ahaideb, M. I. Qureshi, and N. H. Malik, "Statistical evaluation of water tree lengths in XLPE cables at different temperatures," *IEEE Trans. Dielectr. Electr. Insul.*, vol. 11, no. 6, pp. 995–1006, Dec. 2004.
[18] M. Shuvalov, M. Mavrin, V. Ovsienko, and A. Romashkin, "Analysis of water trees in power cable polymeric insulation," *J. App. Poly. Sci.*, vol. 88, pp. 1543–1549, 2003.

Rashed H. Bhuiyan received the B.Sc. and M.Sc. degrees in electrical engineering from the Bangladesh University of Engineering and Technology, Dhaka, Bangladesh, in 2003 and 2005, respectively. He is currently working towards the Ph.D. degree at the Department of Electrical Engineering, University of South Carolina, Columbia, since January 2006.

During his B.Sc. and M.Sc. studies, he published several international conference papers. He also served as a faculty member with the Bangladesh University of Engineering and Technology, Dhaka, from 2003 to 2005. His current research interests include near-field miniature sensor design and wireless communications.

Roger A. Dougal (M'82–SM'94) He received the Ph.D. degree from Texas Tech University, Lubbock, in 1983.

He joined the University of South Carolina in 1983. He is the Thomas Gregory Professor of Electrical Engineering at the University of South Carolina. He is currently Director of the Virtual Test Bed Project, a multidisciplinary, multiuniversity effort to develop a comprehensive design, simulation, and virtual prototyping environment for advanced power sources and systems, integrating power electronics, electromechanics, electrochemistry, and controls into a common testbed. In addition to his interests in modeling and simulation, his expertise also includes power electronics, physical electronics, and electrochemical power sources.

Mohammod Ali (M'93–SM'03) received the B.Sc. degree in electrical and electronic engineering from the Bangladesh University of Engineering and Technology, Dhaka, in 1987, and the M.A.Sc. and Ph.D. degrees, both in electrical engineering, from the University of Victoria, Victoria, BC, Canada, in 1994 and 1997, respectively.

He was with the Bangladesh Institute of Technology, Chittagong, from 1988 to 1992. From January 1998 to August 2001, he was with Ericsson Inc., Research Triangle Park, NC, first as a Staff Engineer and then as a Senior Staff Engineer. Since August 2001, he has been with the Department of Electrical Engineering, University of South Carolina, Columbia, where he is currently an Associate Professor. He had also held appointments as a Visiting Research Scientist with the Motorola Corporate EME Research Laboratory, Plantation, FL, from June to August 2004. He is the author/coauthor of over 90 journal and conference publications and holds five U.S. patents. His research interests include miniaturized packaged (embedded) antennas, metamaterials and their antenna applications, distributed wireless sensors and rectennas, reconfigurable antennas, and portable/wearable antennas and their interactions with humans (SAR).

Dr. Ali is the recipient of the 2003 National Science Foundation Faculty Career Award. He is also the recipient of the College of Engineering and Information Technology Young Investigator Award from the University of South Carolina in 2006.